INTERNATIONAL ATOMIC ENERGY AGENCY
UNITED NATIONS EDUCATIONAL, SCIENTIFIC AND CULTURAL ORGANIZATION
INTERNATIONAL CENTRE FOR THEORETICAL PHYSICS
I.C.T.P., P.O. BOX 586, 34100 TRIESTE, ITALY, CABLE: CENTRATOM TRIESTE

UNITED NATIONS INDUSTRIAL DEVELOPMENT ORGANIZATION

INTERNATIONAL CENTRE FOR SCIENCE AND HIGH TECHNOLOGY

SMR/548-13

Course on Oceanography of Semi-Enclosed Seas
15 April - 3 May 1991

"Shallow Marine Sediment Transport & Deposition"

I.N. McCAVE
University of Cambridge
Department of Earth Sciences
U.K.

Trieste Course on Oceanography of Semi-Enclosed Seas April/May 1991

Shallow marine sediment transport and deposition

Lecture 1. Geological Setting and General Principles.

Lecture 2. Tidal and Wave Driven Transport and Bedforms.

Lecture 3. Sedimentation in the Adriatic Sea.

Lecture 1. (Prof. I.N. McCave)

1. Origin of continental shelves and shallow semi-enclosed seas - e.g. N.Sea, Baltic, Adriatic, Gulf of St Lawrence, Gulf of Paria, Java and Timor Seas, Gulf of Thailand, Yellow Sea and Gulf of Bohai, N. Bering Sea, Persian Gulf, Hudson Bay, Gulf of Tongking, Gulf of Carpentaria, etc. Post-glacial sea-level rise of ~125m since last glacial maximum at 21 ka ago has flooded continental margins. Sea-level has been approximately constant for the last 5 ka..

2. "Relict" sediments are left behind on the shelf resulting from earlier conditions - e.g. beach sands at the shelf edge, river channel sands, drowned coral reefs, deltas and sand banks. These were partly re-worked during rising sea-level.

3. Areas dominated by modern supply are mainly in areas of (a) abundant sediment supply (b) shallow areas nearshore. Many areas of the world have little modern input at all, e.g. N.W. Europe, E.N. America, Africa, Australia. Supply is dominated by a) relief of land, especially near the sea and b) rock weathering.

4. Size of sedimentary materials supplied : Gravel (>2mm), Sand (2 mm - 63μm), Silt (63 μm - 2 μm) Clay (< 2 μm) - sizes are nominal grain diameters. Silt-plus-clay is termed "mud" and is usually cohesive, whereas gravel, sand and pure silt coarser than 10 μm are non-cohesive.

5. Control of material size supplied is again climate (controlling type of weathering, chemical vs. mechanical) and relief (controlling stream velocities and ability to move larger material). Nearshore sediment size reflects latitude (climate).

6. Basic transport properties of materials are shown by behaviour at incipient motion (critical) conditions, and mode of transport after critical conditions are exceeded. (a) for <u>non-cohesive</u> material the critical erosion stress can be experimentally defined as f (size) for uniform sized material on a flat bed; mixed sizes on rippled beds are more difficult to specify. (b) for <u>cohesive</u> sediment there is not yet agreement on a single parameter that defines the behaviour of the material under a given stress; some people think the yield strength of the material to be a good parameter.

7. When moving, material may be supported by continuous or intermittent contact with the bed, "bed load", or by the action of fluid turbulence, "suspended load". Various arguments lead to the conclusion that the bedload flux ($ML^{-1}T^{-1}$) is proportional to shear stress to the power 3/2, or flow speed cubed. Suspended load flux is to a higher power, exactly what is uncertain, in the range of flow speed to the fourth or fifth power. This steep power dependence confers great importance on relatively rare events of great magnitude such as large storms.

8. Under uniform flow with increasing speed ripples appear on the bed soon after critical conditions, and at higher flow speeds larger periodic

transverse bedforms termed dunes occur. Ripples scale in height and wavelength on the grainsize of the material whereas dunes scale on the dimensions (height) of the flow. These bedforms constitute the boundary roughness offered by the bed to the flow. At higher stress dune bedforms can be washed out and the bed becomes flat again.

9. In suspension transport the sediment is distributed with height above the bed according to the ratio $w_s/\kappa u_*$ where w_s is the still-water settling velocity of the particles, u_* is the shear velocity $(\tau_0/\rho)^{\frac{1}{2}}$ and κ is von Karman's constant (0.4). For medium sand and coarser (> 250 μm, w_s > 3 cm/s) suspended sediment is concentrated in the lower few metres of the water column. Finer sediment is more uniformly distributed.

10. Fine cohesive sediment behaviour in suspension is affected by the fact that it can flocculate or be aggregated by biological agencies and so form multiple units of greater settling velocity than their components. Because collision frequency goes up with concentration, settling velocity also rises - to a maximum of about 0.2 cm/s. Aggregates also break up in the high shear zones close to the boundary. The settling velocity distribution thus varies according to the state of shear in the flow.

11. Sediment deposition occurs for bedload at stresses a little below the critical movement condition when it simply stops rolling. We can define a critical deposition condition for suspended load, which is thought to be equivalent to the critical erosion condition for non-cohesive material of the same settling velocity, but transport can continue for some time below critical deposition conditions because the water column takes a while to clear, the precise time depending on height of water column, boundary shear stress and particle settling velocity.

These controls lead to a huge range of sediment types and bedforms in shallow seas. Their occurrence is complicated by the range of variability shown by water movements on time scales from seconds to seasons.

Lecture 2. (Prof. I.N. McCave)

1. Tidal currents: M_2 and M_4 components and their superposition. Modelled boundary stress distributions. Inequalities of peak stress on ebb and flood tides leading (in general) to net sand flux in the direction of maximum stress.

2. Tidal bedforms: occurrence where tidal reworking of the bed is constant and thus dominates wave effects; with increasing flow ripples, sand waves (dunes), sand ribbons and sand banks. Tidal and sediment flows associated with each type, for ribbons $\lambda/h \approx 4$, for banks $\lambda/h \approx 250$ (λ = bedform spacing, h = water depth).

3. Fine sediment transport by tides: net flux in direction of net water flux (differs from sand), action of tidal currents in trapping sediment nearshore in tidal flat areas and estuaries.

4. Wave-driven sediment transport: the problem of a rapidly fluctuating stress and the application of sediment transport formulations for steady flow to time averaged oscillatory flow with a weak superimposed current. Empirical results for wave-driven transport near-shore. New

results showing differing transport directions of mean $\langle \bar{U}\,\bar{C} \rangle$ and wave-fluctuating $\langle \bar{U}_w \bar{C}_w \rangle$ components, (U is flow velocity, C is sediment concentration, subscript w denotes waves).

5. Wave-generated bedforms: mainly ripples of various sorts, their stability fields and transition to flat bed at high stress.

6. A simple magnitude/frequency approach to wave driven transport and the definition of areas of shelves dominated by sand and mud when under active modern sediment input.

7. Shelf sediment facies and the overall control of the distribution of gravel, sand and mud resulting from glacial history, sea level change, sediment supply, wave and tidal current dispersal.

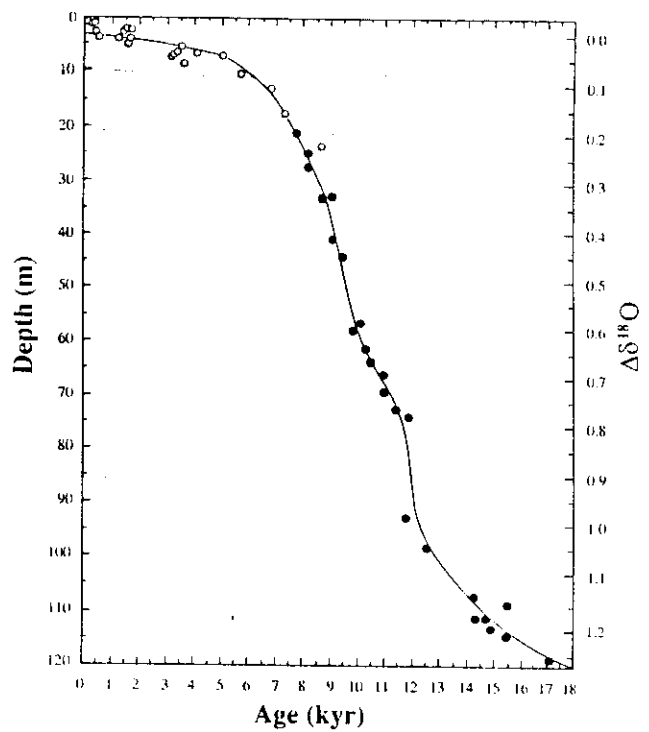

FIG. 2 Barbados sea level curve based on radiocarbon-dated *A. palmata* (filled circles) compared with *A. palmata* age-depth data[1] (open circles) for four other Caribbean island locations. All radiocarbon ages in this figure are corrected for local seawater $\Delta^{14}C$ by subtracting 400 yr from the measured radiocarbon ages[8] but they are not corrected for secular changes in atmospheric ^{14}C levels[15]. The Barbados data are corrected for the estimated mean uplift of 34 cm kyr^{-1}. The right-hand axis of the Barbados sea level curve (solid line) is scaled to the estimated $\delta^{18}O$ change of mean ocean water using the calibration in ref. 5.

Fairbanks,
Nature 1989

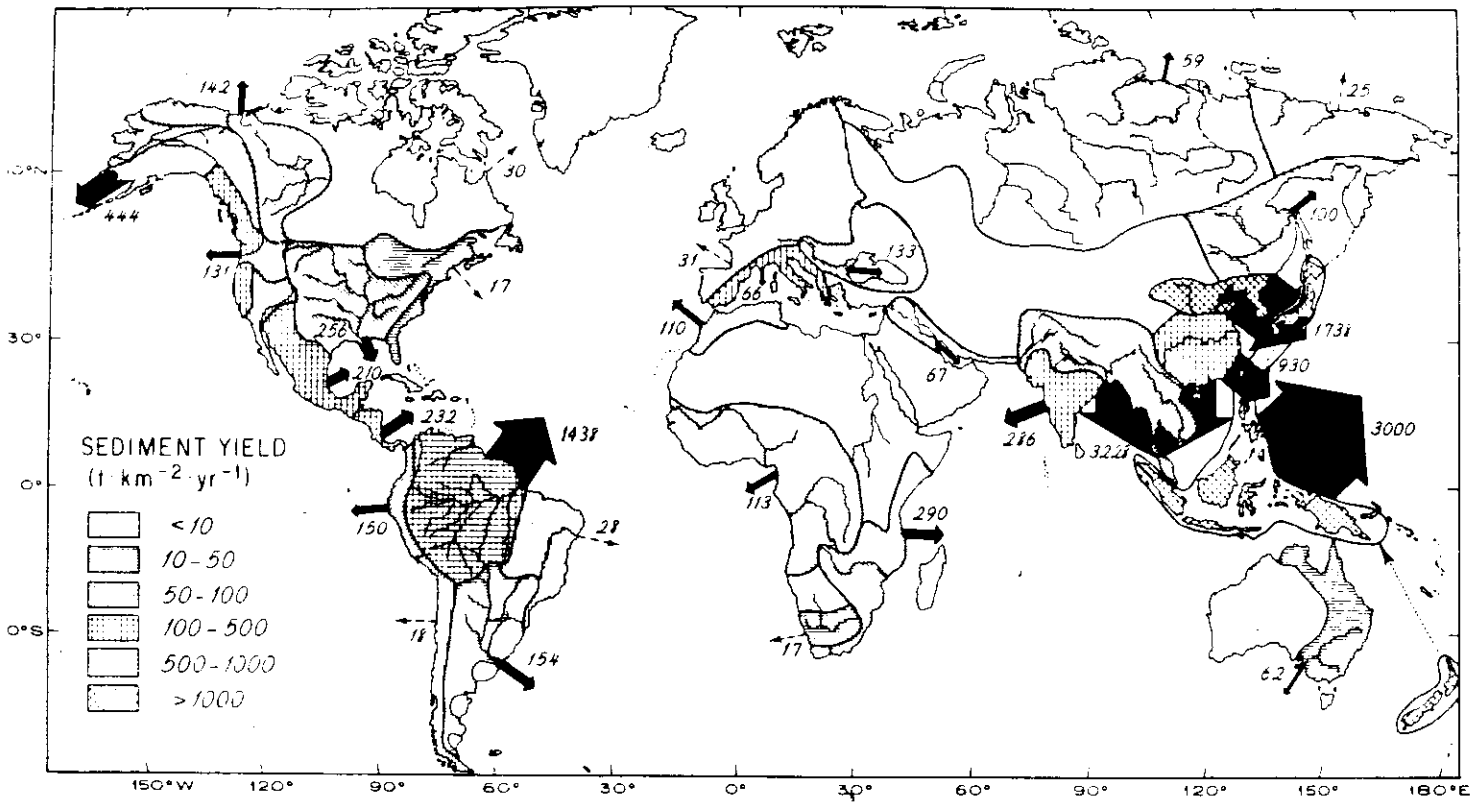

FIG. 4.—Annual discharge of suspended sediment from various drainage basins of the world; width of arrows corresponds to relative discharge. Numbers refer to average annual input in millions of tons. Direction of arrows does not indicate direction of sediment movement. The sediment yields and major rivers of the various basins also are shown; open patterns indicate essentially no discharge to the ocean.

Milliman & Meade. (1983) J. Geol.

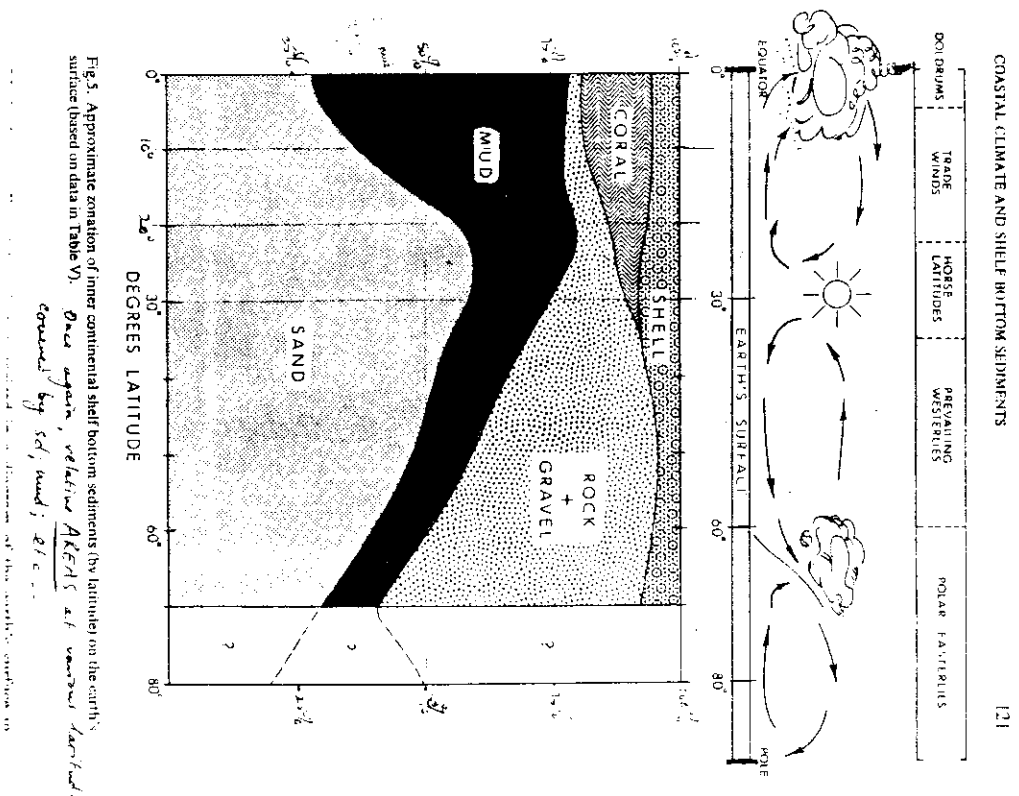

Fig. 5. Approximate zonation of inner continental shelf bottom sediments (by latitude) on the earth's surface (based on data in Table V).

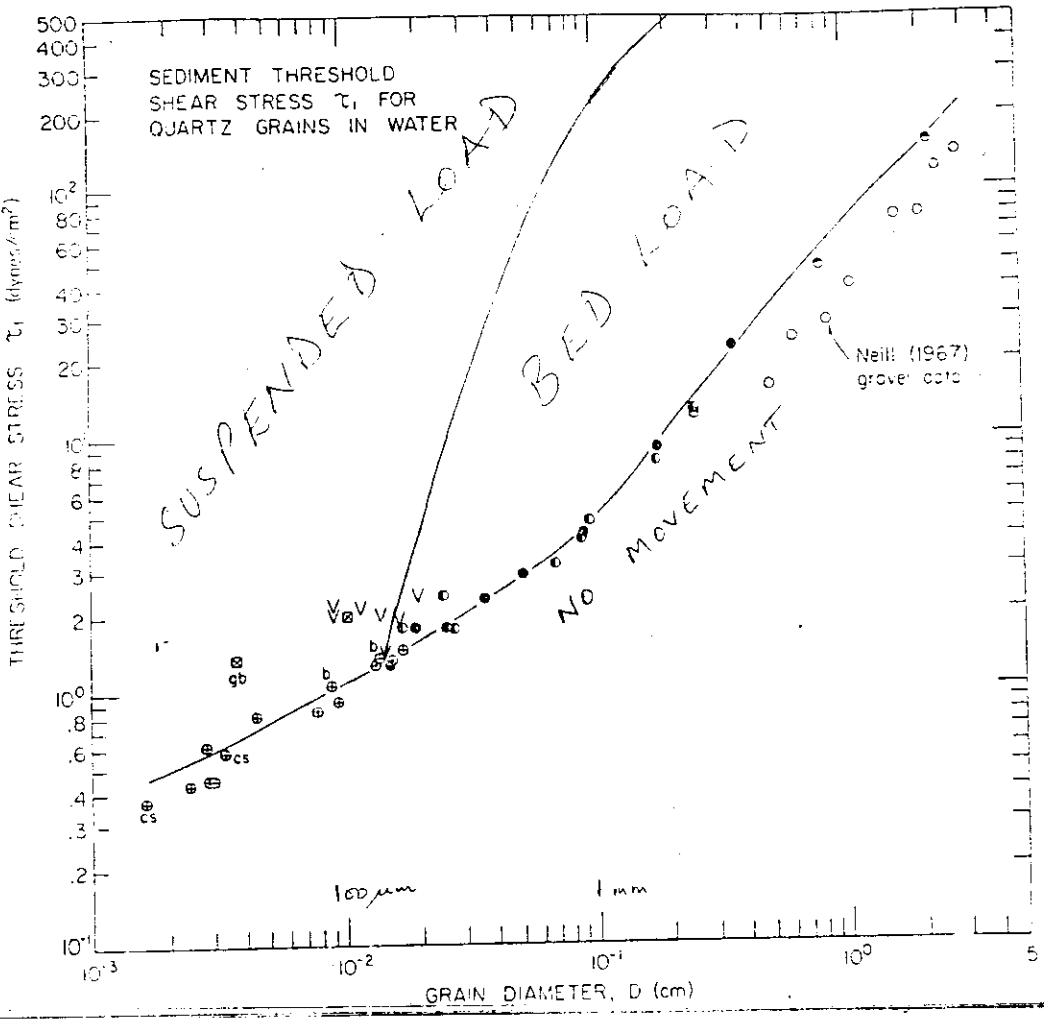

Critical erosion condition for sand and gravel

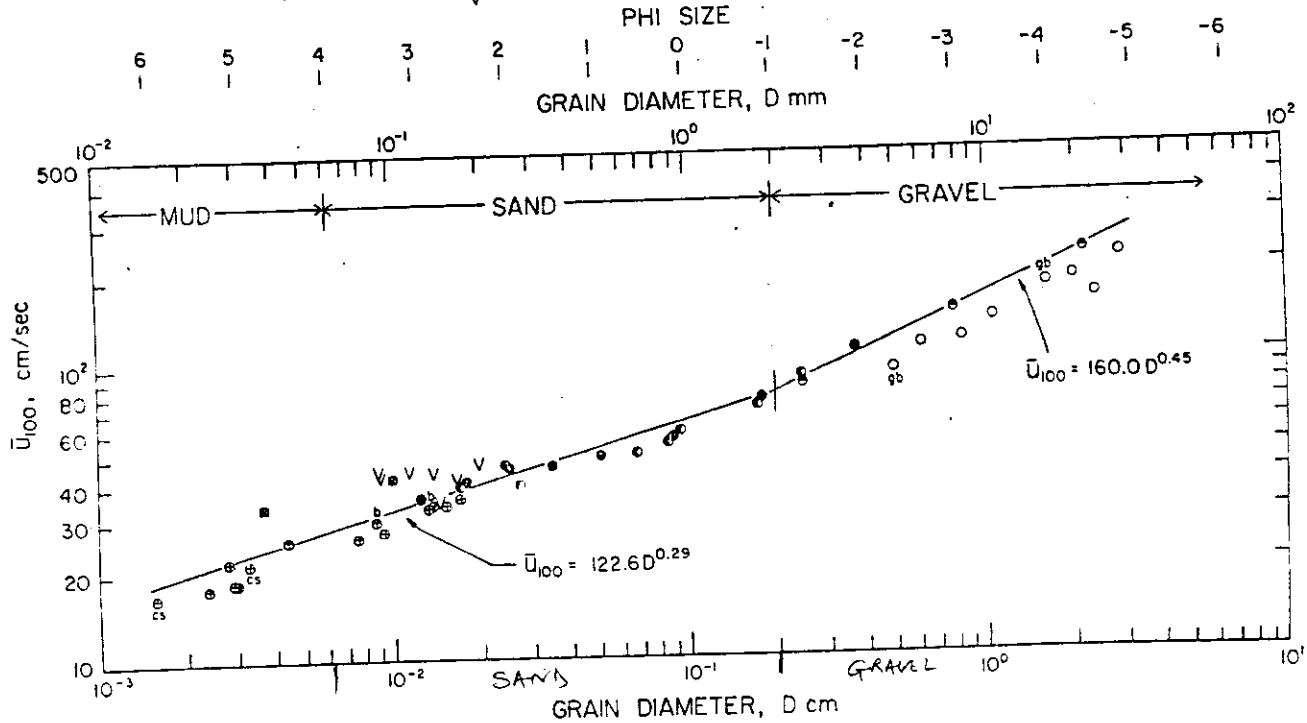

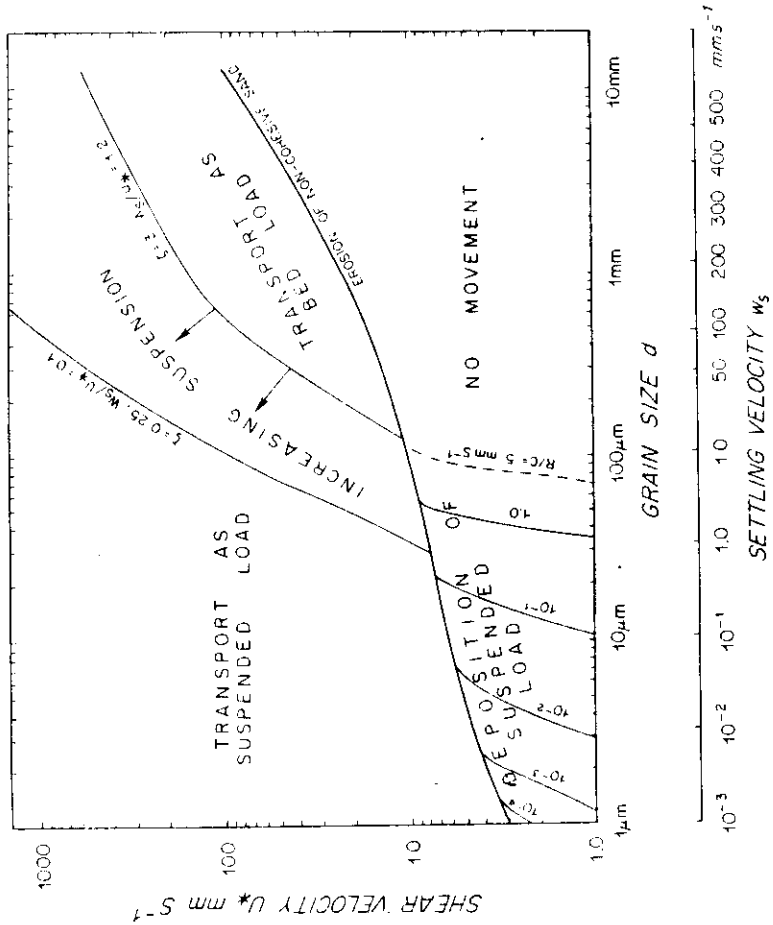

Critical erosion constrictions for mud.

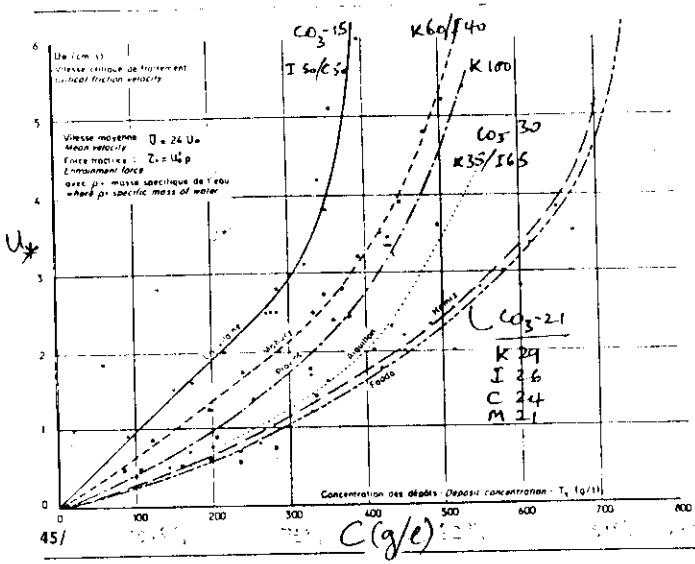

I = Illite
C = Chlorite
K = Kaolinite
M = Montmorillonite (Smectite).

45/ Vitesses critiques d'érosion de différentes vases.
Critical scour velocity for various muds.

46/ Variation de la vitesse d'érosion en fonction de la concentration.
Scour velocity vs. concentration.

47/ Variation de la vitesse d'érosion en fonction de la rigidité initiale.
Scour velocity vs. initial rigidity.

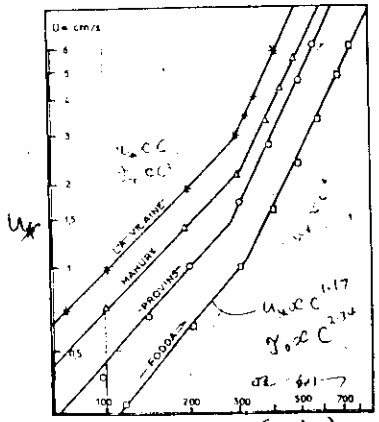

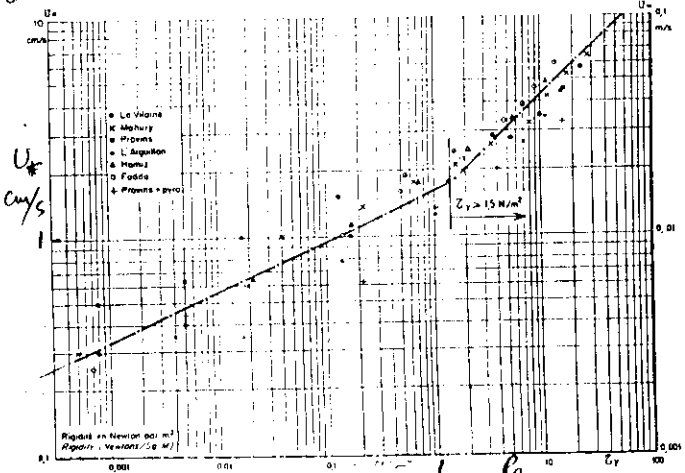

yield strength

CONTROL OF SAND WAVE OCCURRENCE

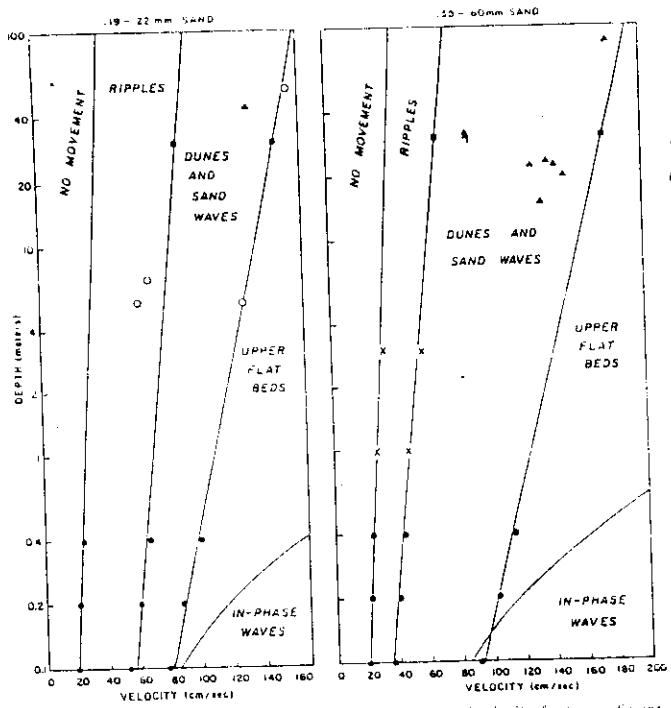

Fig. 8. Semi-log plots of bed phase as a function of depth and velocity for two sediment-size ranges. Triangles and open circles represent San Francisco Bay sand-wave fields and flat-appearing beds, respectively; squares are points on bed-phase boundaries in Fig. 10. Solid circles are points measured or interpolated from bed-phase boundaries determined by Southard (1975, figs. 2-2, 2-3, and 2-5). Crosses and circled dots are points on bed-phase boundaries determined by Boothyroyd and Hubbard (1975) and Dalrymple et al. (1978), respectively. Flume velocities are depth-averaged for steady flows; bay velocities are depth-averaged for peak flow during average tides.

from Rubin & McCulloch (1980)

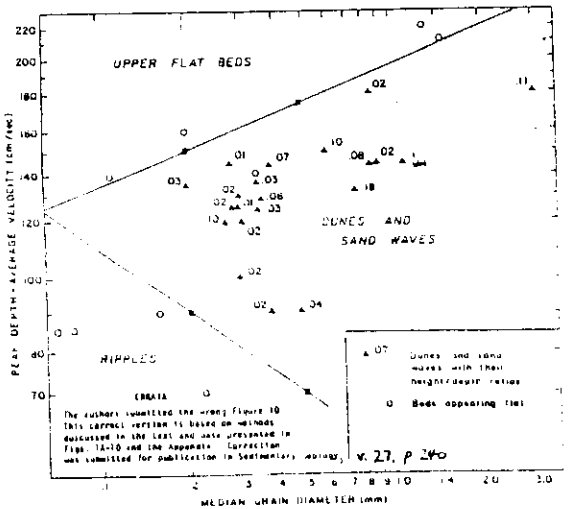

from Rubin & McCulloch erratum notice: Mar Geol 7, 27: 240

Fig. 10. Log-log plot of bed phase as a function of sediment size and velocity for flow

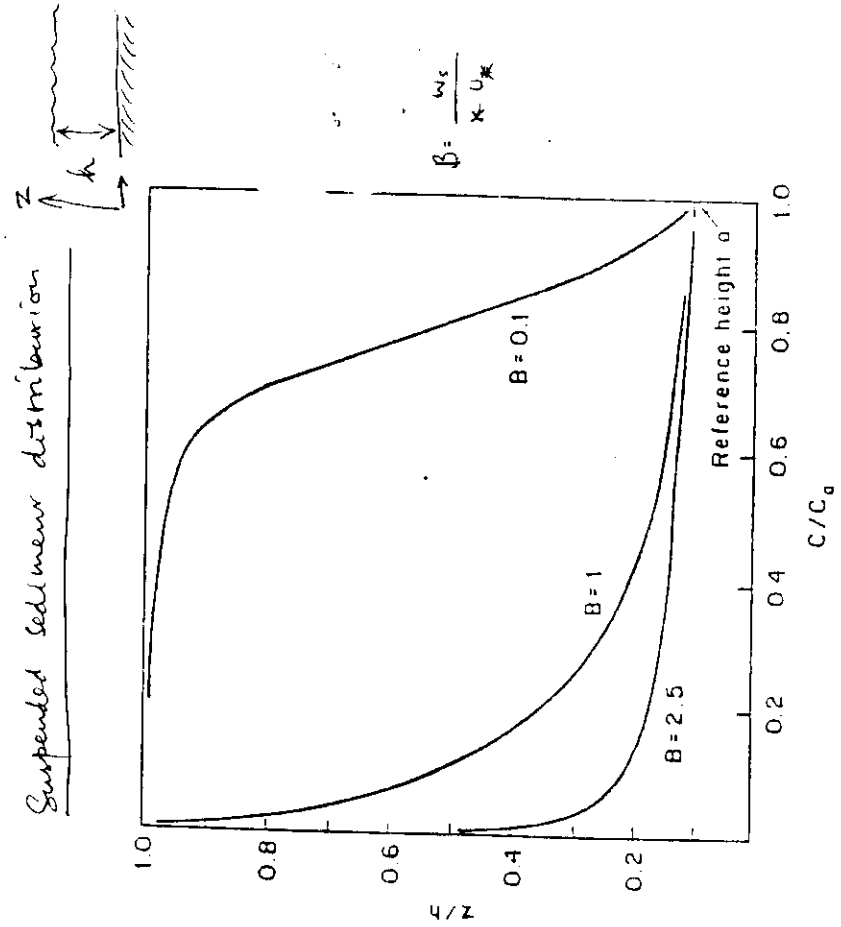

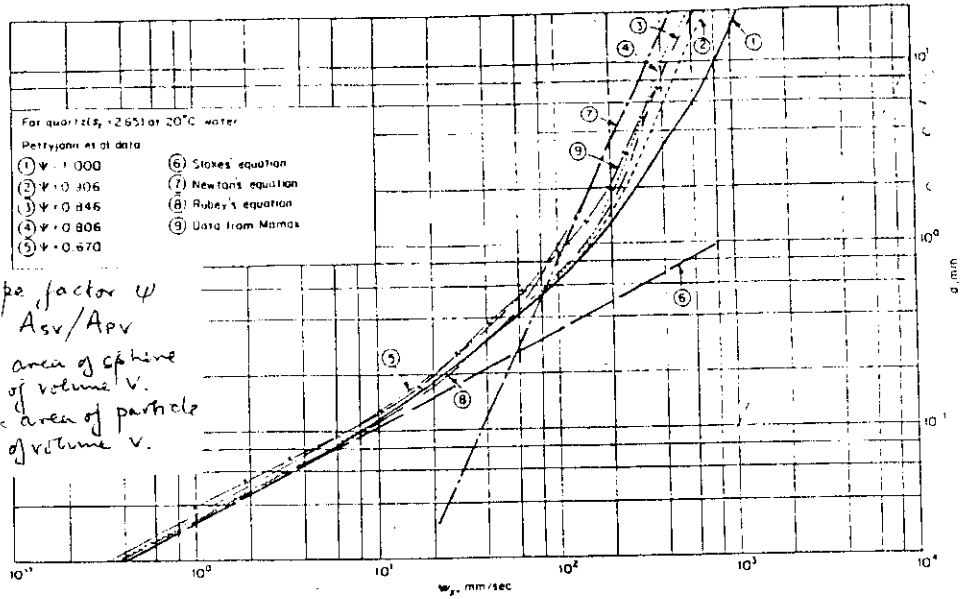

shape factor ψ
$= A_{sv}/A_{pv}$
A_{sv} = area of sphere of volume V.
A_{pv} = area of particle of volume V.

Fig. 4.4 Settling velocity vs. particle diameter; various equations and shape-factor parameters Ψ. [*After* GRAF *et al.* (1966).]

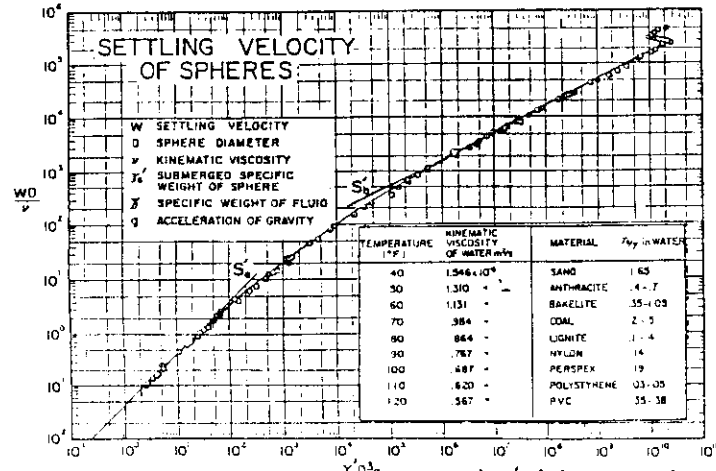

FIG. 3.2

D = grain diameter
w = w_s = settling velocity

$\left(\frac{\gamma_s' D^3}{\rho \nu^2}\right) = \frac{4}{3}$ (gains dimensionless parameter for critical motions)

Settling velocity of solid spherical particles

Settling velocity of mud aggregated particles

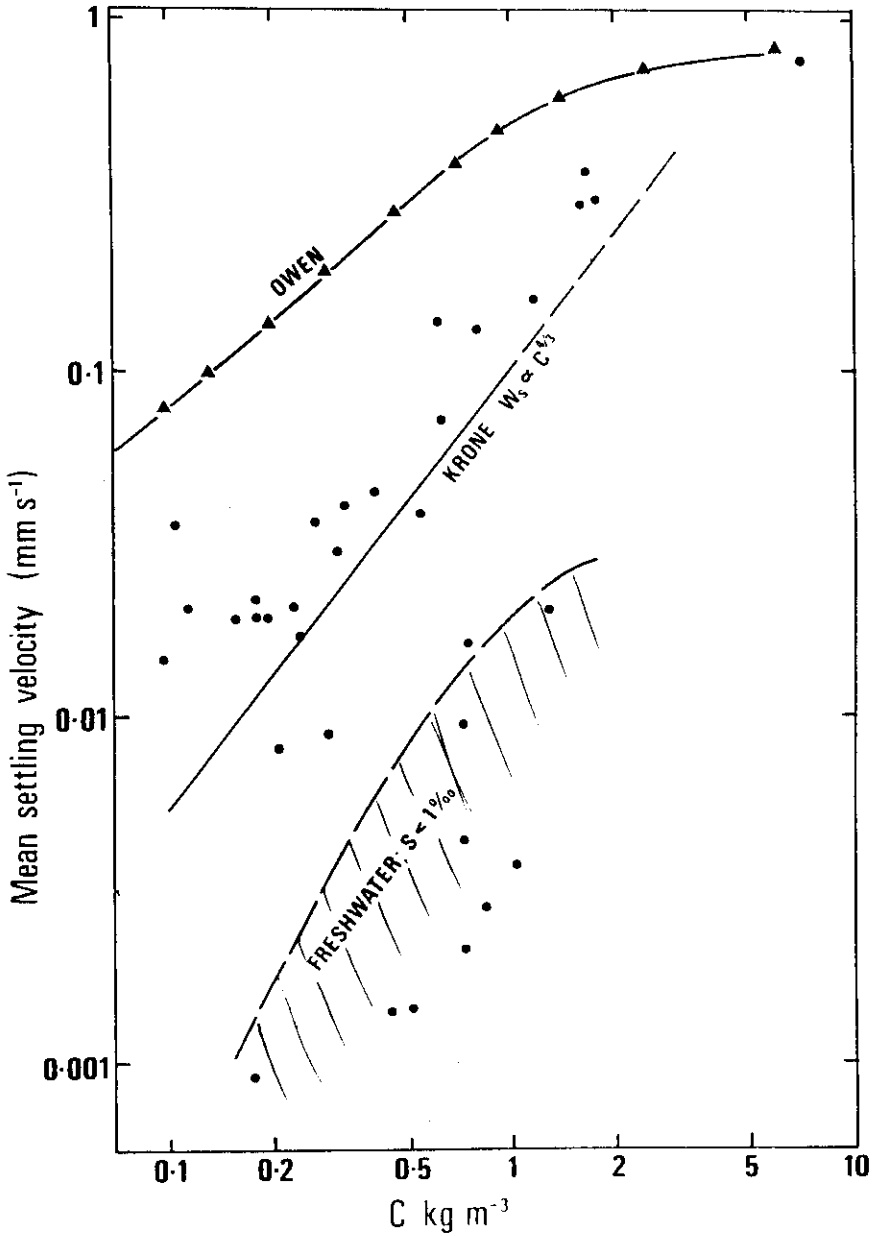

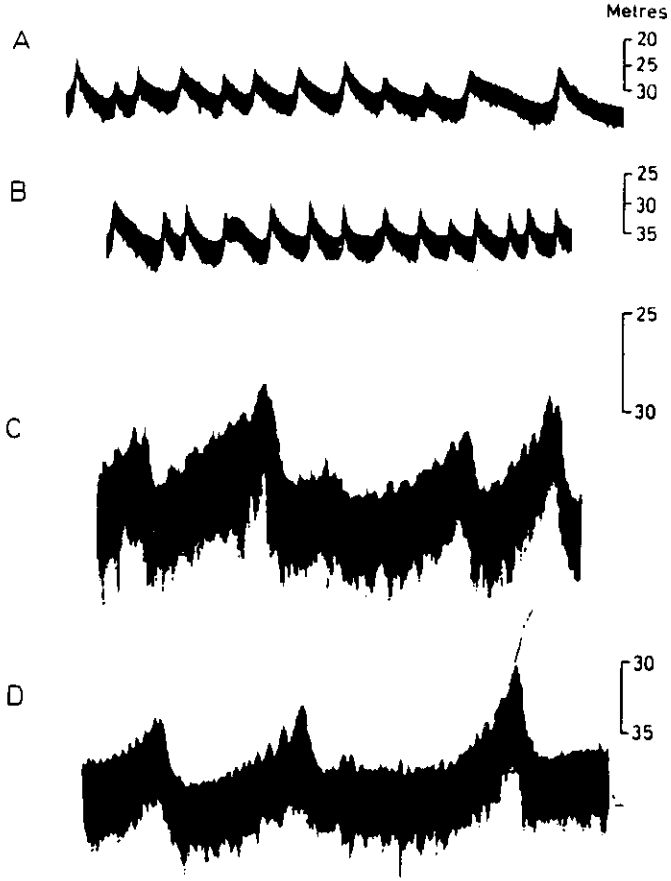

Fig.5. Examples of sand waves in the Southern Bight in the region of 52°30'N 03°15'E. The scales on the right also give water depth. Profiles A, B, and the last wave on D show the increase in slope of the stoss side towards the crest. The fourth wave from the left of section B is a pronounced "cat-back" form, while the second from the right of section A is a weakly developed one. Section C and especially D illustrate sand waves with megaripples, and their increase in size to the sand-wave crest. Approximate lengths of section are: A = 3,800 m; B = 2,800 m; C = 900 m; D = 1,200 m.

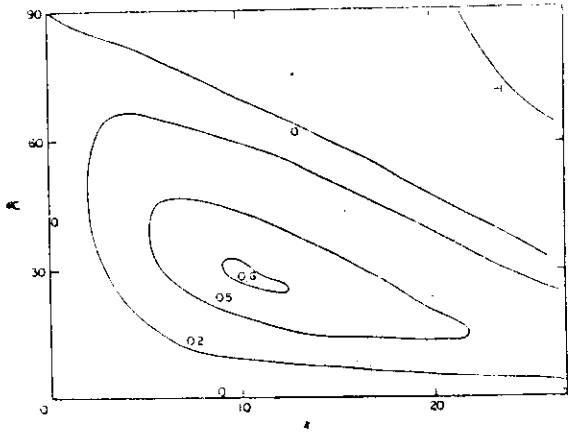

Figure 2. Contours of growth rate $\sigma_0(k,a)$ as a multiple of $SU^3Fn/2(s-\rho)gH$ when $f = 0$, $F = 1$, $\lambda = 0.005$, $m = 2 = n$. Since $f = 0$ there is symmetry between positive and negative inclinations a.

from Huthnance (1982a)

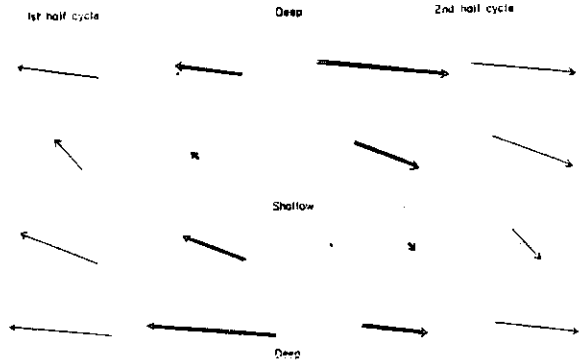

Figure 4. Sand-bank growth mechanism. Inclination a is negative as for Norfolk Sandbanks. →: current, ⇒: transport.

from Huthnance (1982a)

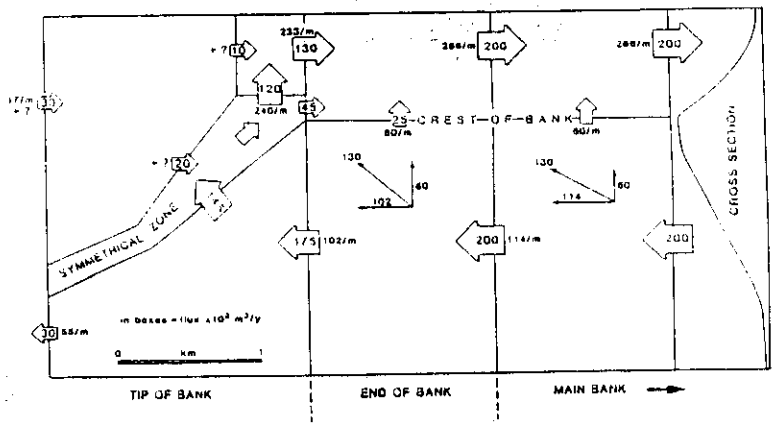

Fig. 14. Box model of sand circulation around the end of Haisborough Sand. Fluxes in boxed arrows are annual values in thousands of m^3 passing across the side of the box which they cut. Fluxes written alongside arrows are values of m^2 m-width^{-1} y^{-1}. The two vector diagrams are labelled with fluxes as m^3 m^{-1}.

from McCave & Langhorne (1982)

(3)

BANK ORIENTATION, SPACING and SAND CIRCULATION

Maximum growth is at an angle between bank axis and tidal flow of about 28°.

$k = \frac{2\pi H}{CL}$, H = bank height, L = spacing and C = drag coefficient, assumed ~ 0.0025.

The maximum at $k \sim 1$ gives $L \sim 250\,H$.

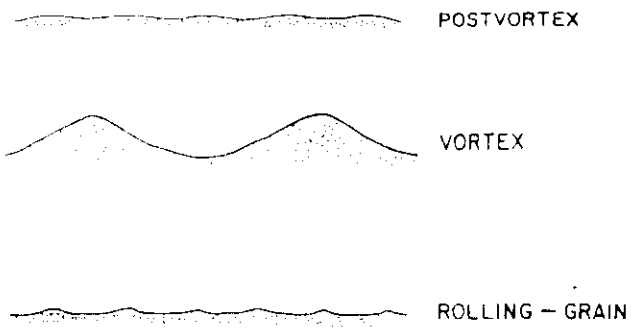

Figure 2-9. Typical normal-to-flow profiles of the various types of oscillation ripples.

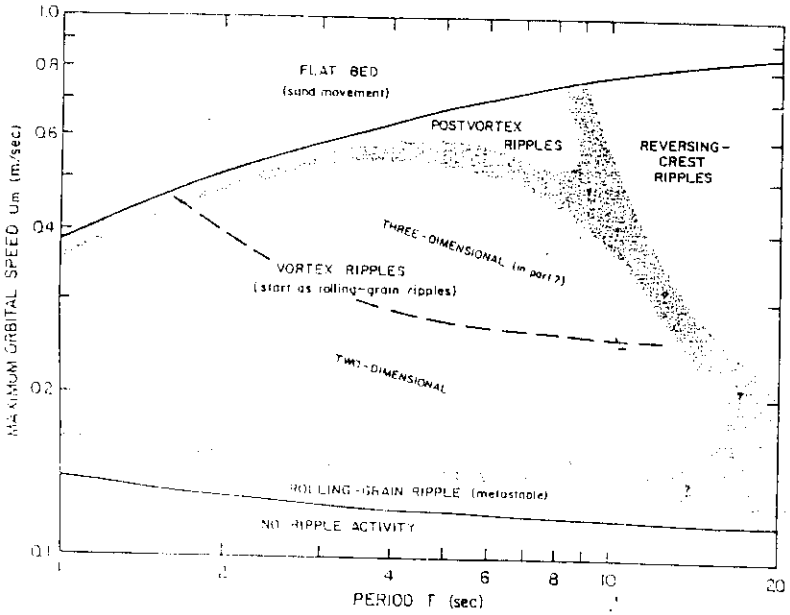

Figure 2-14. Schematic plot of kinds of oscillation ripples as a function of maximum orbital speed and oscillation period T for sand sizes of 0.15-0.21 mm. Shaded areas are partly transition zones and partly areas of

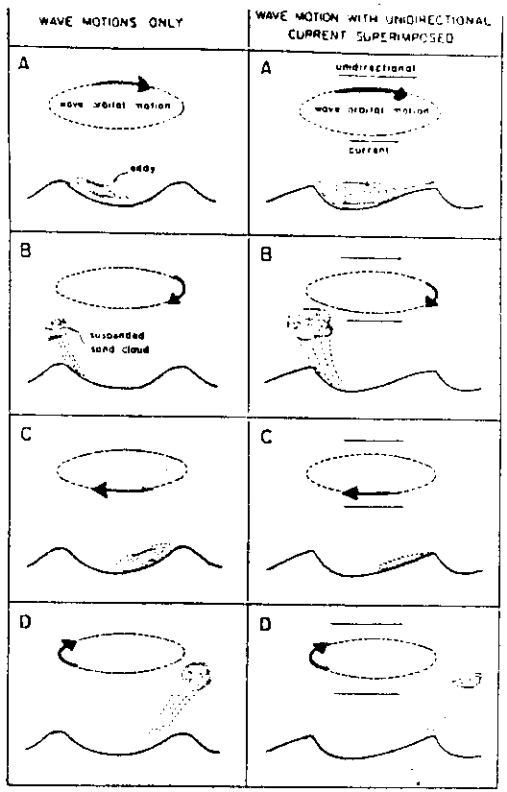

FIGURE 9. *Sediment suspension due to eddies formed in protective lee of ripple crests, without and with unidirectional currents superimposed on the wave motions. With a superimposed onshore current the ripples become asymmetric so that more sediment is thrown into suspension in an offshore direction, as shown, giving an unexpected offshore sediment transport. From Komar (in press).*

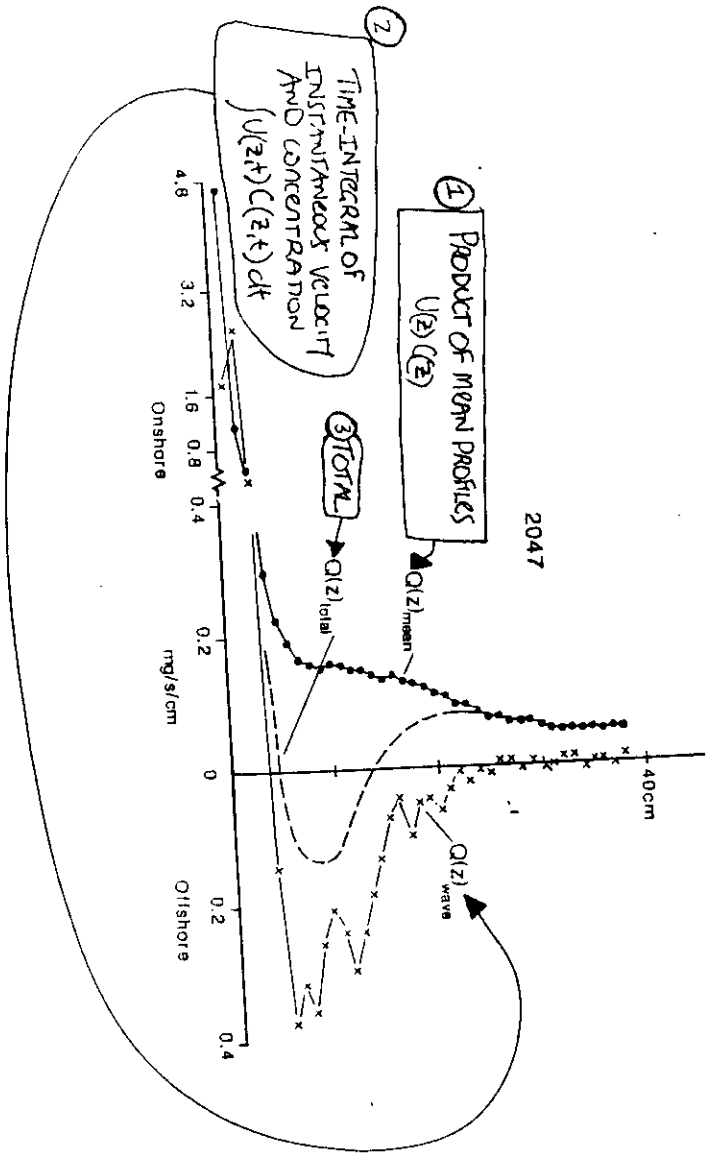

WAVE EFFECTIVENESS

(McCave, J Sed Petrol. 19
Pickrill, Mar. Geol. 198

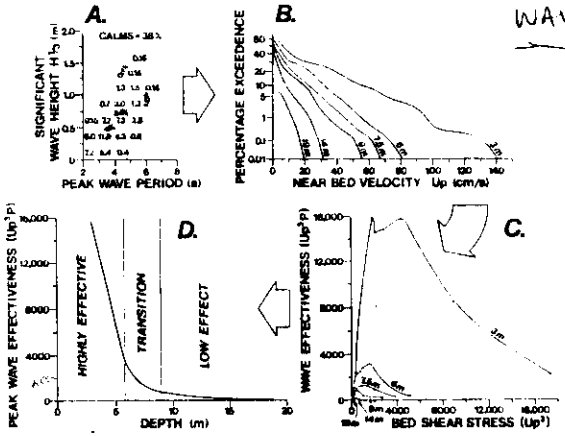

Fig.7. An example of the steps in the derivation of peak wave effectiveness, French Creek. (A) Plot of significant wave height against peak wave period; (B) Percentage exceedance curves of near-bed velocities for water depths of 3, 6, 7.5, 9, 14 and 19 m; (C) The distribution of wave effectiveness at the bed versus bed shear stress; (D) Peak wave effectiveness (from each curve in C) plotted as a function of depth.

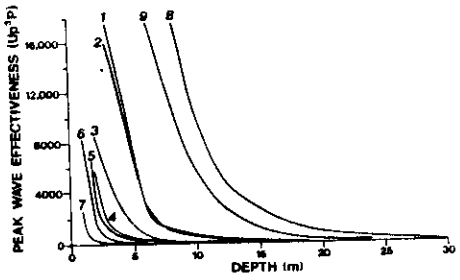

Fig.8. Peak wave effectiveness plotted as a function of depth. Numbers 1–6 refer to wave-rider stations in Fig.1; Station 7 = Lake Manapouri, New Zealand; 8 = Toronto, Lake Ontario; 9 = Battle Island, Lake Superior.

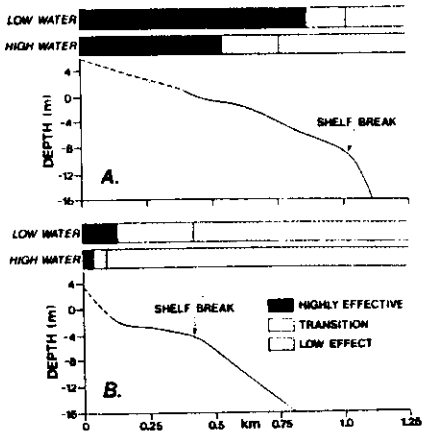

Fig.11. Tidal translation of peak wave effectiveness zones across the terrace. (A) High-energy terrace at French Creek (47; *EF* = 46 km) with a tidal range of 5.0 m. (B) low-energy terrace at Cordova Bay (24, *EF* = 12 km) with a tidal range of 3.8 m (wave data from Lund).